

## Simultaneous mesospheric gravity wave measurements in OH night airglow emission from Gadanki and Kolhapur – Indian low latitudes

R. N. Ghodpage<sup>1</sup>, A. Taori<sup>2,\*</sup>, P. T. Patil<sup>1</sup> and S. Gurubaran<sup>3</sup>

<sup>1</sup>Medium Frequency Radar, Indian Institute of Geomagnetism, Shivaji University Campus, Kolhapur 416 004, India

<sup>2</sup>National Atmospheric Research Laboratory, Gadanki 517 112, India

<sup>3</sup>Equatorial Geophysical Research Laboratory, Indian Institute of Geomagnetism, Tirunelveli 627 011, India

**Simultaneous photometric measurements of mesospheric OH night airglow emissions have been made from two stations, Gadanki (13.5°N, 79.2°E) and Kolhapur (16.8°N, 74.2°E), India during February–March 2010 to study the differences in the observed wave characteristics. Our results reveal the wave periodicities to be similar at both locations, which ranged from 2 to 8 h. The inferred Krassovsky parameters ( $\eta = |\eta|e^{i\phi}$ ) show large variability, with ranges of  $|\eta|$  varying from 2.4 to 4.2 over Gadanki and from 2.2 to 6.3 over Kolhapur. The phase values of Krassovsky parameter,  $\phi$ , exhibit variation from  $-101^\circ$  to  $-202^\circ$  in Kolhapur data and  $-38^\circ$  to  $-93^\circ$  in Gadanki data. The deduced vertical wavelengths indicate that the observed waves were propagating upwards with vertical wavelengths varying from  $-26$  to  $-62$  km. We note that the observed night-time OH emission profile shows the peak of emission at  $\sim 85$  km in Kolhapur and at  $\sim 90$  km in Gadanki in the corresponding months. These observed characteristics of waves and the cause of noted differences are discussed.**

**Keywords:** Airglow emissions, low latitudes, mesospheric gravity, wave measurements.

THE temporal variations of mesospheric OH night airglow intensities and rotational temperatures are known to be caused by the passage of gravity waves and tides of lower atmospheric origin. At mesospheric altitudes, amplitudes of these waves and tides become so large that they govern the observed variability in mesospheric wind and temperature fields. There are several reports that study the long as well as short-period wave features with the help of mesospheric airglow emissions. For example, Takahashi *et al.*<sup>1</sup> report the detection of planetary waves; Taylor *et al.*<sup>2</sup> and Taori *et al.*<sup>3</sup> report tidal features. Apart from these long-period waves, there are several reports on the short-period gravity wave features at mesospheric altitudes<sup>4–7</sup>. In particular, the photometric measurements can be utilized to characterize the dynamical features by Krassovsky analysis<sup>8</sup>, which relates the percentage inten-

sity changes to the associated temperature. The Krassovsky parameter is a complex quantity explained as

$$\eta = |\eta|e^{i\phi}, \quad (1)$$

where the magnitude of  $\eta$  is defined as

$$|\eta| = \frac{\delta I / \bar{I}}{\delta T / \bar{T}}, \quad (2)$$

where  $\delta$  represents the amplitude of the wave perturbation in intensity ( $\bar{I}$ ) and temperature  $\bar{T}$  and the over bar of the quantity is the time-averaged mean for that wave perturbation.  $\phi$  is the phase difference between intensity ( $\phi_I$ ) and temperature ( $\phi_T$ ) waves and is defined as follows.

$$\phi = \phi_I - \phi_T, \quad (3)$$

(i.e. a negative  $\phi$  means temperature wave leads the intensity wave). Further, the vertical wavelength ( $\lambda_z$ ) can also be estimated using the calculated  $\eta$  and  $\phi$  values as described by Tarasick and Hines<sup>9</sup>.

There are several cases of isolated wave event characterization using the Krassovsky analysis at OH emission altitudes<sup>10–16</sup>. However, only few of them are from low and equatorial latitudes that provide the Krassovsky parameters with respect to the wave periodicity (ranging from 0.5 to 12 h). One of them is by Viereck and Deehr<sup>17</sup> spanning the wave-period ranges 1–20 h, and by Reisin and Scheer<sup>18</sup> who focused mainly on the semidiurnal tidal fluctuations. These efforts have been further extended by Lopez-Gonzalez *et al.*<sup>19</sup> with the help of spectral airglow temperature imager (SATI) measurements. Recently, Ghodpage *et al.*<sup>20</sup> have observed waves having period between 2 and 12 h, which propagate upward from the measurements of the O(<sup>1</sup>S) 557.7 nm and OH(7,2) band from a low-latitude station, Kolhapur, during 2004–2007 in night airglow data. It is important to note that simultaneous mesospheric OH measurements with the aim to compare the Krassovsky parameters from different low-latitude stations have not been done so far. We planned a campaign from Gadanki (13.5°N, 79.2°E) and Kolhapur (16.8°N, 74.2°E) stations in the Indian sector to monitor mesospheric OH emissions during the period February–March 2010 (as these months are known to provide more optically clear night sky compared to other months). The aim of the present study is to provide additional information on Krassovsky ratio from the Indian sector and also to investigate that observed differences in wave characteristics in terms of Krassovsky parameters.

The instrumentation used in the present study is as follows. The mesosphere lower thermosphere photometer (MLTP) uses narrow bandwidth (FWHM  $\sim 0.4$  nm) interference filters (5 cm diameter) having high transmission coefficients (40–70%) and low temperature coefficient

\*For correspondence. (e-mail: taori@narl.gov.in)

( $\sim 0.012 \text{ nm}/^\circ\text{C}$ ) to monitor OH(6–2), O<sub>2</sub>(0–1), O(<sup>1</sup>D) and O(<sup>1</sup>S) emissions. The MLTP has full field-of-view of 4°. All the filters are mounted in a filter wheel (housed in a temperature-controlled chamber), which is rotated to insert the desired filter into the optical path. In this study an observation cycle consists of 10 sec integrations repeating each filter at 90 sec interval. The MLTP uses Hamamatsu H7421-50 photomultiplier module as the detector which has wide spectral response ( $\sim 160\text{--}900 \text{ nm}$ ) and peak cathode sensitivity of  $\sim 4 \times 10^6$  at 840 nm. Cooling with the help of Hamamatsu C8137 ensures a low dark count  $\sim 150$  counts/sec at 0°C. The detector sampling is synchronized with the filter rotation through a trigger. A menu-driven computer software is used for ascertaining the above control operations and data-saving. Details of MLTP with initial results and validation are discussed elsewhere<sup>21,22</sup>. The photon counts recorded are then used to estimate the mesospheric temperature by ratio method as described by Meriweather<sup>23</sup>. The errors in the temperature estimates (caused by uncertainty in the spectroscopic constants and instrumental limitations) are not more than 5%, which gives a temperature precision of  $\sim 2 \text{ K}$ . In the present study the MLTP was pointed towards zenith and only mesospheric OH emission measurements are utilized.

The multi-spectral photometer measures night airglow emissions at OH(8,3), O(<sup>1</sup>D) and O(<sup>1</sup>S) wavelengths near simultaneously. The utilized interference filters (10 cm diameter) have full width at half maximum  $\sim 1 \text{ nm}$ . These filters have transmission efficiency  $\sim 30\text{--}65\%$  at 24°C and a low temperature coefficient ( $\sim 0.018 \text{ nm}/^\circ\text{C}$ ). The integration time for each emission monitoring is 10 sec. The field-of-view of the photometer is 10°. As the stepper motor rotates, a filter wheel keeps each filter in the field-of-view one by one. At the beginning and after the end of each rotation, the filter wheel is brought to the home position which further aligns the filters in the field-of-view. The stepper motor rotation and home position sensing are controlled by the computer. The photomultiplier tube, EMI9658B is used as detector. A high-gain transimpedance amplifier is used in the signal amplification in order to convert the weak (in the range of nA) output current of the photomultiplier into corresponding voltage form. Output is further recorded in the computer in analogue format in terms of arbitrary units along with time. Because the aim of the present study is to compare the mesospheric wave characteristics, only OH measurements are presented.

We carried out a coordinated campaign during February–March 2010 to compare the gravity wave characteristics from Gadanki and Kolhapur. Owing to the tropical latitude behaviour only two common nights with clear sky conditions were available for detailed analysis, when more than 5 h of observation could be made. We present these observations and results in the following paragraphs.

To quantify the wave parameters observed in the data, a simple best-fit cosine model<sup>3</sup> is utilized and the periodicity, phase and amplitude of wave perturbation in the data are estimated for intensity and temperature data independently. The modelled best-fit solutions are then used to get the amplitude and phase information of the dominant oscillations. For example, the nocturnal variability of temperature and intensity data noted on 8–9 March 2010 over Gadanki is shown in Figure 1, where Figure 1 *a* plots the mean temperature deviations (normalized to their mean temperature values) and Figure 1 *b* plots the mean intensity deviation (normalized to their mean intensity values). The connecting lines in the plots show the normalized mean deviations in Figure 1 *a* and *b*, and the filled circles show 0.5 h averaged data on which the best-fit analysis was carried out. The solid red lines in each plot show the best-fit results. To elaborate that the best-fitted wave represents our data sample, plotted together in dashed purple lines and dotted blue lines are forced-fitted values for shorter and longer period waves than the best-fitted periodicity. We can see that only best-fitted  $\sim 5.9 \text{ h}$  wave represents our nocturnal variability and hence we conclude that the  $\sim 5.9 \text{ h}$  wave is dominant in temperature and intensity data with amplitudes  $\sim 4.5\%$  and  $16.5\%$ . Further to find the second dominant wave in our data, we subtract the best-fit model data from the normalized mean deviation data to obtain the residuals. These 0.5 h averaged data of residual temperature and intensity data are shown in Figure 1 *c* and *d* respectively. The solid red lines show the best-fit results for the residual variability. It is clear that in the residual data, dominant waves in temperature and intensity data have a periodicity of  $\sim 2.4$  and  $2.6 \text{ h}$  respectively.

When it comes to Kolhapur data (Figure 2), the mean of airglow intensity is 1.6 arbitrary units and temperature data are 202.2 K. Similar to Figure 1, Figure 2 shows the mean deviations of mesospheric temperatures (Figure 2 *a*) and intensity (Figure 2 *b*) normalized to their mean values over Kolhapur with respect to local time for 8–9 March 2010 observations. The solid red lines in each plot show the results of the best-fit cosine model. The presence of  $\sim 5.2$  and  $5.8 \text{ h}$  waves is noteworthy in the nocturnal temperature and intensity variability, with amplitudes  $\sim 2\%$  and  $10\%$  respectively. The residuals from the best-fit model data (deviations) that provide information on the second dominant wave in the nocturnal data are plotted in Figure 2 *c* and *d*. These show the nocturnal variability for residual temperature and intensity data respectively. The best-fit analysis reveals the presence of  $\sim 2.8$  and  $3.1 \text{ h}$  waves respectively, in the temperature and intensity residuals.

While comparing the wave parameters obtained from Gadanki and Kolhapur, although the occurrences of similar waves should be ascertained with parameters such as horizontal and vertical wavelengths, in the absence of these values we assume that similar wave period observation

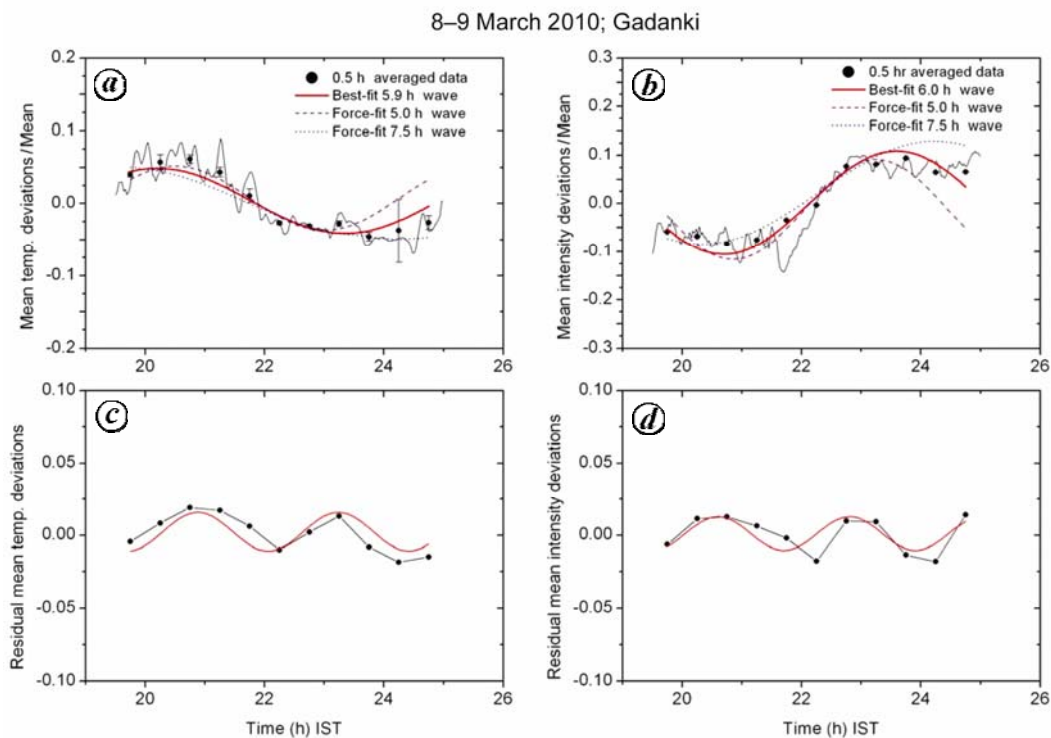


**Figure 1.** Nocturnal variability in the mesospheric OH emissions during 8–9 March 2010. (a) and (b) plots the mean deviations in temperature and intensity data normalized to their mean values, whereas (c) and (d) show their residual variability obtained by removing the cosine model fitted data. Filled circles show the 0.5 h averaged data. Solid red lines in each plot show the result of best-fit cosine model which estimates the dominant wave periodicity, amplitude and phase of waves in the data obtained over Gadanki, while the purple dashed and blue dotted lines show the forced oscillations. It is noteworthy that best-fitted model closely follows the 0.5 h average data.

emphasizes the presence of similar wave events at both locations. Note that both (nocturnal and residual) dominant wave periods on 8–9 March 2010 show a similar periodicity over Gadanki and Kolhapur. This obviously signifies a large latitudinal extent of these waves, which is similar to the results obtained by Taori and Parihar<sup>21</sup>. It is interesting to note that Gadanki data show further shorter wave periodicities to exist, which are not present in the Kolhapur data. Partially, this may be due to the higher temporal resolution of Gadanki data. Temporal resolution is poor in the Kolhapur data because in this period, multi-spectral photometer over Kolhapur was operated in meridian scanning mode and as cautioned by Hines and Tarasick<sup>24</sup>, we have only used zenith observation to calculate the Krassovsky parameter. Therefore, we avoid discussions on the observed shorter period waves over Gadanki.

Figures 3 and 4 show the nocturnal variability observed in Gadanki and Kolhapur data on 10–11 February 2010. The legends to these figures are the same as described in earlier cases. It is noted that the Gadanki data on this night reveal the presence of 7.5 and 2.6 h wave periods with the relative intensity and temperature perturbation amplitudes for the dominant longer-period wave to be  $\sim 2.5\%$  and  $1\%$  respectively. The Kolhapur data also show the dominant wave periods to be  $\sim 8.0$  and  $4$  h. The

relative intensity and temperature perturbation amplitudes for the dominant long-period wave over Kolhapur are  $\sim 13.5\%$  and  $2.1\%$  respectively. It is important to state that small differences in wave periodicity do not necessarily mean a different wave because of complex dynamical conditions at mesospheric altitudes. On 10–11 February 2010, the residual temperature and intensity data show the presence of  $\sim 2.6$  h wave over Gadanki. One may also note large amplitudes of short-period waves with  $\sim 0.6$  h periodicity. Regarding the differences in the observed wave periods at Gadanki and Kolhapur, it is possible that the nonlinear interaction between the prevailing short-period waves over Gadanki may have a role, of which we are unsure. Further, regarding the long-period wave, the possibility of tidal aliasing cannot be ruled out because of limited night-time measurements. However, as the best-fit results suggest, the 0.5 h averages of the observed data are well represented by the best-fitted wave and therefore, most often it is the shorter wave periods which are not well accounted in the best-fitting. Therefore, we believe that our deduced wave periodicity, amplitude and phases are very close to the true oscillation parameters observed on these particular nights.

The waves observed at OH altitudes can be characterized with the help of amplitude ratio and phase difference between intensity and temperature waves (eqs (1) and (2)).

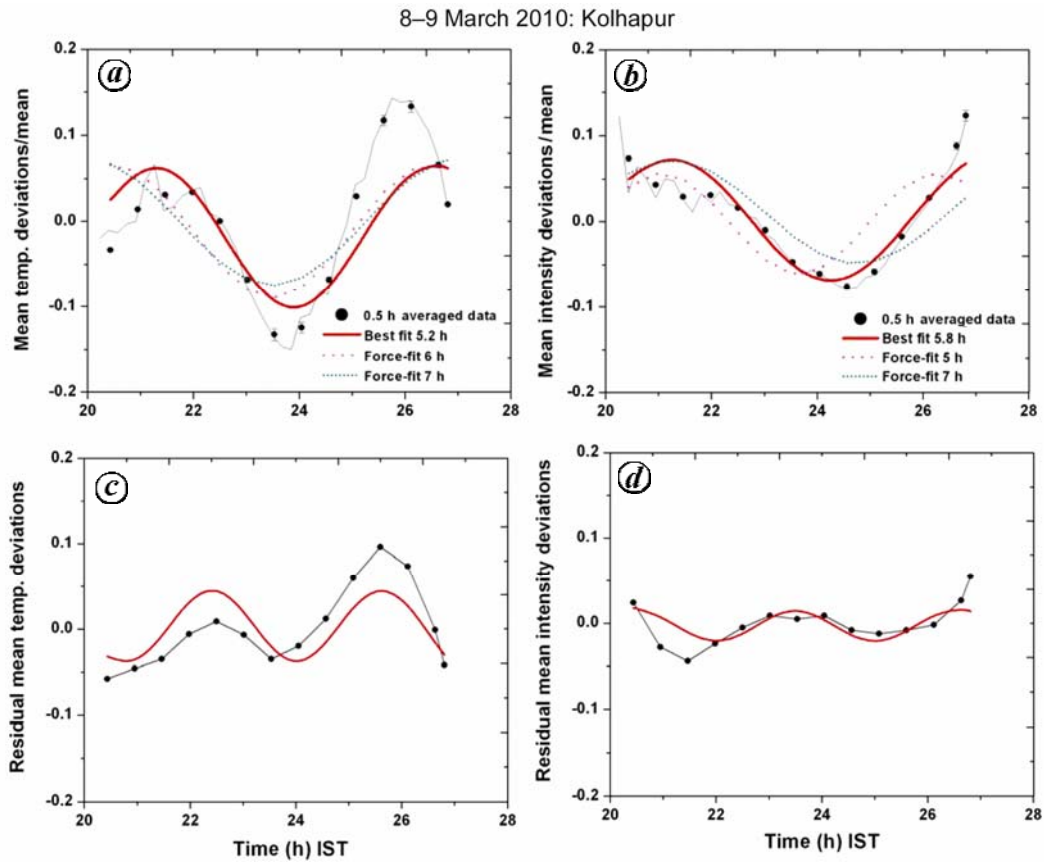


Figure 2. Same as Figure 1, but for Kolhapur data.

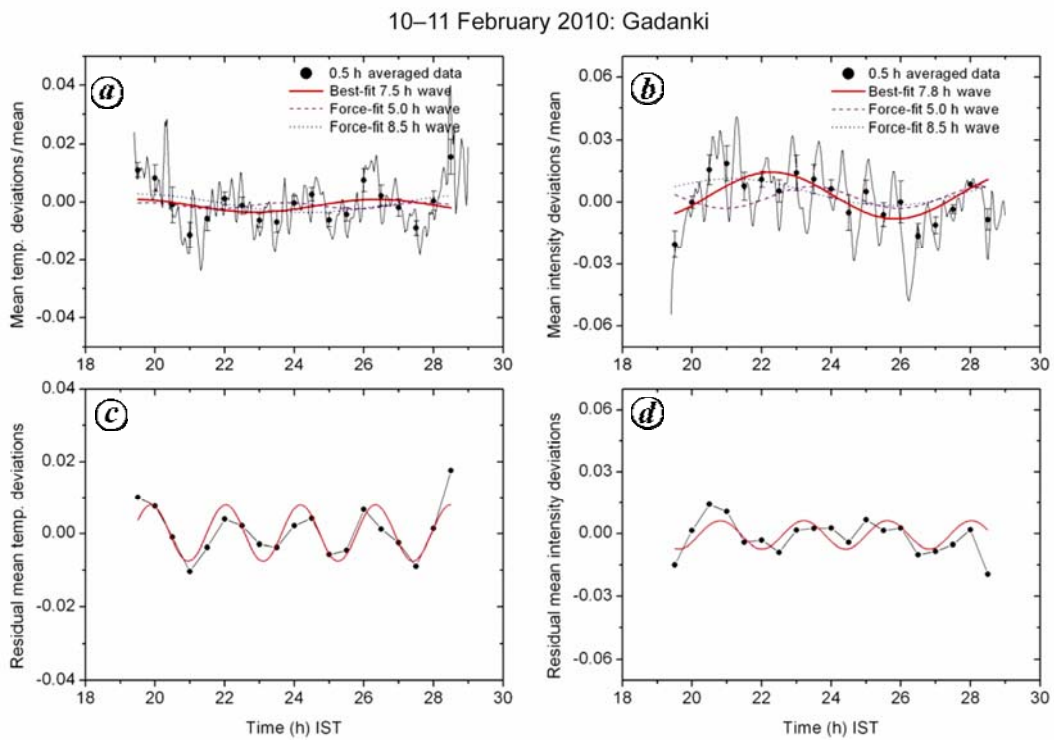


Figure 3. Same as Figure 1, but for 10–11 February 2010.

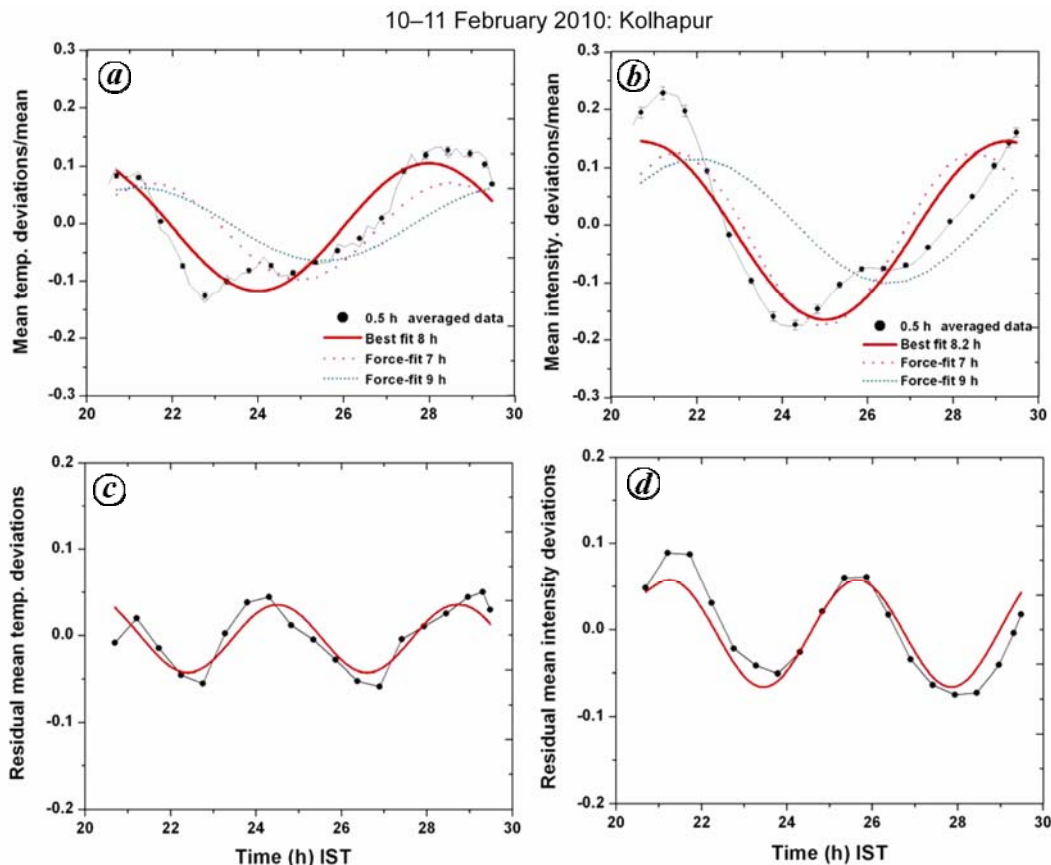


Figure 4. Same as Figure 2, but for 10–11 February 2010.

The amplitude of Krassovsky ratio  $\eta$  represents the transfer function for a wave to convert the intensity perturbations into temperature<sup>25,26</sup>. Normally, this ratio ranges from  $\sim 0.5$  to 12 with the least number for dissipating or trapped waves<sup>27,28</sup>. We utilize amplitudes normalized to the mean values of intensity and temperature data to calculate the Krassovsky ratio.

In Figure 1, we note that dominant long-period wave has periodicity  $\sim 5.9$  h with amplitudes  $\sim 8.4$  K and 990 counts in temperature and intensity data respectively. The mean temperature and intensity values were  $\sim 208.4$  K and 6218 counts respectively. This results in  $|\eta|$  of  $\sim 3.6$ . The phase difference between intensity and temperature waves was obtained with the cross-correlation analysis of the best-fitted waves. The phase of the waves over Gadanki was  $\sim 23.2$  and  $21.5$  h for temperature and intensity data respectively, which results in a phase difference of  $\sim 1.7$  h in intensity and temperature wave, i.e.  $\phi$  value of  $-101 \pm 30^\circ$ . Similarly, for shorter period (periodicity  $\sim 2.4$  h), the  $|\eta|$  and  $\phi$  values are found to be  $\sim 2.9$  and  $-109 \pm 25^\circ$ . On this night, corresponding observations from Kolhapur (Figure 2) reveal the temperature and intensity waves to have amplitudes of  $\sim 2.3$  K and 0.11 arbitrary units respectively. Further, Kolhapur data reveal the phase of temperature and intensity waves to occur at  $\sim 23.1$  and  $24.3$  h IST. These result in  $|\eta|$  of  $\sim 5$  and

$\phi \sim -82 \pm 32^\circ$ . Similarly, the shorter-period wave over Kolhapur exhibited  $-58 \pm 24^\circ$  and 2.2 to be the phase and amplitude of the Krassovsky parameter respectively.

On 10–11 February 2010, we note the long-period wave to exhibit a periodicity  $\sim 7.5$  h (Figure 3). The dominant long-period wave amplitudes over Gadanki are  $\sim 0.8$  K and 92 photon counts for temperature and intensity data with their mean values  $\sim 200$  K and 5849 counts. This results in  $|\eta|$  values  $\sim 4.2$ . The phase  $\phi$  value for this wave was found to be about  $-141 \pm 40^\circ$ . The long-period wave in Kolhapur data had periodicity of  $\sim 8$  h for which the amplitudes are estimated to be  $\sim 2$  K and 12.6% for temperature and intensity data respectively, with mean values  $\sim 202.4$  K and 2.2 arbitrary units, i.e.  $|\eta| \sim 6.3$ . The phase  $\phi$  is estimated to be  $-38 \pm 20^\circ$ . One may note the significant difference in the Krassovsky parameters for long-period waves in Gadanki and Kolhapur observations. The short-period wave over Gadanki has a periodicity of  $\sim 2.6$  h, whereas the Kolhapur data show the short-period wave to be of  $\sim 4$  h periodicity, which seems to be significantly different. However, as stated earlier, because of the presence of a short-period 0.6 h wave in Gadanki data, the possibility of nonlinear wave–wave interaction cannot be ruled out, which we are unsure of at present. The short-period wave over Gadanki (2.6 h wave period) shows the  $|\eta|$  and  $\phi$  values to be  $\sim 2.4$  and

**Table 1.** Derived wave parameters of Kolhapur and Gadanki data with standard errors

Date	Gadanki				Kolhapur			
	Wave period (h)	$ \eta $	$\varphi$ (degree) $\pm$ error	$\lambda z$ (km) $\pm$ error	Wave period (h)	$ \eta $	$\varphi$ (degree) $\pm$ error	$\lambda z$ (km) $\pm$ error
8 March 2010	5.9	3.6	$-101 \pm 30$	$-58 \pm 20$	5.2	5.0	$-82 \pm 32$	$-60 \pm 26$
8 March 2010	2.4	2.9	$-109 \pm 25$	$-47 \pm 28$	2.8	2.2	$-58 \pm 24$	$-43 \pm 18$
10 February 2010	7.5	4.2	$-141 \pm 40$	$-62 \pm 12$	8.0	6.3	$-38 \pm 20$	$-50 \pm 20$
10 February 2010	2.6	2.4	$-202 \pm 45$	$-49 \pm 23$	4.0	3.6	$-93 \pm 38$	$-26 \pm 12$

$-202 \pm 45^\circ$  respectively, whereas these values for the short-period wave over Kolhapur ( $\sim 4$  h wave period) are calculated to be  $\sim 3.6$  and  $-93 \pm 38^\circ$  respectively. Table 1 summarizes the calculated values of the Krassovsky parameters over Gadanki and Kolhapur. There are differences in the observed wave magnitudes which may be due to (i) the altitude differences of observations at two locations, (ii) highly variable mesospheric wave dissipation processes, and/or (iii) the multi-wave-mode coupling processes. The Krassovsky parameters, being sensitive to the above, are a suitable tool for these studies.

Overall, the  $|\eta|$  values vary from  $\sim 2.4$  to  $4.2$  over Gadanki and  $\sim 2.2$  to  $6.3$  over Kolhapur. The  $\varphi$  values, on the other hand, reveal large differences and vary from  $-101^\circ$  to  $202^\circ$  over Gadanki and  $-38^\circ$  to  $-93^\circ$  over Kolhapur. Further, we also estimate the mean vertical wavelength  $\lambda z$  with the help of  $|\eta|$  and  $\varphi$  values, which vary from  $-50$  to  $-62$  km for long wave period over Kolhapur and Gadanki. In case of short-period waves, the vertical wavelengths vary from  $-26$  to  $-49$  km. Comparisons of the deduced wave parameters are shown in Table 1. It is interesting to note that the deduced vertical wavelength values compare well with those reported by Guharay *et al.*<sup>11,29</sup>. It is worth mentioning here that theoretical work of Hines and Tarasick<sup>24</sup> suggests that negative values represent the upward propagating gravity waves and hence our observations reveal that on both nights we noted upward propagating waves.

As mentioned above, the deduced Krassovsky parameters show large differences from one night to another, indicating a highly dynamical mesosphere; a fact which other workers have also demonstrated. For example, Reisin and Scheer<sup>12</sup> found mean values of  $|\eta| = 5.5 \pm 0.6$  and  $\varphi = -66^\circ$  for OH. In a further report by the same authors<sup>18</sup>, based on 5-year observations, they found the mean  $|\eta|$  of  $\sim 5.6$ , although they mention that for waves of periodicity 1000 sec to 3 h,  $|\eta|$  is  $\sim 3.4$ . In another study, based on long-term observations with a spectral airglow temperature imager (SATI) from a mid-latitude station, Lopez-Gonzalez *et al.*<sup>19</sup> reported a mean  $|\eta|$  of approximately  $\sim 8.6$  for the OH data (with very large variability). Guharay *et al.*<sup>29</sup> found that for wave periods varying from 6 to 13 h,  $|\eta|$  varies from  $\sim 1.7$  to  $5.38$  and the phase varies from  $-13^\circ$  to  $-90^\circ$ . Similarly, Aushev *et al.*<sup>10</sup> show the amplitude of Krassovsky parameters (for wave periods

ranging from 2.2 to 4.7 h) to vary from 2.4 to 3.6 and phase to vary from  $-63^\circ$  to  $-121^\circ$ . It is noteworthy that our values broadly agree with those of Guharay *et al.*<sup>11,29</sup>, Reisin and Scheer<sup>12,18</sup> and Viereck and Deehr<sup>17</sup>, whereas they are somewhat different from the values reported by Lopez-Gonzalez *et al.*<sup>19</sup>.

Of relevance to the observations is the fact that there is large scatter within different reports with no consensus in the calculated Krassovsky parameters. There may be various reasons for the observed differences between various reports. One of the possible causes may be due to the oxygen profile variability<sup>30</sup> from one station to another as the  $|\eta|$  depends on [O] profile and complex OH chemistry<sup>25</sup>. Another cause could be the quenching of molecular lines by collision with perturbed molecules during the transitions from different vibration levels<sup>31</sup>. Also, an altitude difference of OH layer from one location to another may be responsible for the observed differences. At the same time, variation in the background wind conditions may also alter the deduced parameters. In particular, Makhlof *et al.*<sup>31</sup> attempted to account for the  $\eta$  characteristics by modifying Hines' model and using a new photochemical dynamical model (PDM); but were unable to explain the appearance of the negative phases. Hines and Tarasick<sup>24</sup> found a wide range of  $\eta$  variability. Further, Hines and Tarasick<sup>32</sup> discussed the necessary correction for thin and thick layer approximations for the calculation of  $\eta$  from airglow emissions due to gravity waves interaction. They also pointed out that OH emission intensity, which affects the derived  $\eta$ , does not depend on the oxygen profile and other minor species; which contradicts the existing theory<sup>25,30,33</sup>. In short, there is no single accepted theory for the observed variability in Krassovsky parameters and investigators have been showing large ranges of  $\eta$  and  $\varphi$  values. In the present study, we also note that the observed vertical wavelength (VW) values of Gadanki and Kolhapur data show large differences from one night to another (Table 1). The mean VW for long-period nocturnal wave varies from  $-60$  ( $-58$ ) to  $-50$  ( $-62$ ) km in Kolhapur (Gadanki) data from one night to another. Similarly, the VW for the short-period wave varies from  $-43$  ( $-47$ ) km to  $-26$  ( $-49$ ) km in Kolhapur (Gadanki) data from one night to another. We note that the mean VW values for long and short-wave values are larger over Gadanki in comparison to the

Kolhapur data. We can also compare of VW values with existing reports. For example, Reisin and Scheer<sup>18</sup> found a mean VW of approximately  $-30$  km (with  $40$  km variability), which is somewhat in agreement with our values, whereas there are significant differences from the VW values ( $-10$  to  $-20$  km) reported by Lopez-Gonzalez *et al.*<sup>19</sup>. Takahashi *et al.*<sup>15</sup> reported the VW values to vary from  $20$  to  $80$  km, which is in agreement with our results. More recently, Ghodpage *et al.*<sup>20</sup> analysed the long-term nocturnal data of 2004–2007 and also observed that the VW lies between  $-28.6$  and  $-163$  km. Our results are in agreement with this reported value of VW.

One may argue that the observed differences in Krassovsky parameters may be because of different seasons and years. In the present study, we note larger values of  $\eta$  over Kolhapur data compared to the Gadanki data for long wave on similar dates, which indicates a larger intensity to temperature perturbation ratio over Kolhapur during the passage of the wave. This could be due to the differences in the dynamical processes between Kolhapur and Gadanki. We believe that as the gravity wave amplitudes grow exponentially with height, a difference in the peak emission altitude may give rise to such noted differences. To identify this, in Figure 5 we plot the OH volume emission rate profile for these locations (obtained from the SABER instrument on-board the thermosphere ionosphere mesosphere energetic and dynamics (TIMED) satellite). The selected latitude–longitude grids are  $9^\circ\text{N}$  to  $19^\circ\text{N}$  and  $74^\circ\text{E}$  to  $84^\circ\text{E}$  for Gadanki and  $11^\circ\text{N}$  to  $21^\circ\text{N}$  and  $69^\circ\text{E}$  to  $79^\circ\text{E}$  for Kolhapur. The criteria for the selection of SABER data are such that: (i) the SABER pass should be during typical observation times (i.e. nighttime); (ii) the SABER pass should be available at both the

latitude and longitude and (iii) it should not be twilight time. Note that the SABER pass over Kolhapur was at about  $23.7$  IST, while over Gadanki it was at about  $03$  IST (i.e.  $27.2$  IST). Such a night happened to be 18 February 2010 (Figure 5). We can observe that the altitude of OH layer at Kolhapur is near  $85$  km, while over Gadanki it is approximately  $90$  km. The cause of such a variability in OH emission profile may be due to the ozone and water vapour availability at mesospheric altitudes and their latitudinal variations. More studies on this aspect and that the OH emissions may have a systematic latitudinal variability are beyond the scope of the present study. We assume that the observed differences in Krassovsky parameters may be because of this, which may play an important role by affecting oxygen profile as well as quenching. This indicates the importance of the altitude variation of airglow emissions while making an inter-comparison from one station to another and from one season to another.

In conclusion, our results show that though observed wave periodicities were same over Gadanki and Kolhapur, the amplitude and phase of the derived Krassovsky parameters show significant differences. We show that the representative SABER profile indicates a difference in OH emission altitudes which may possibly be the cause of such observations. More data are needed to carry out a wider study to provide further insights into the characterization of the waves.

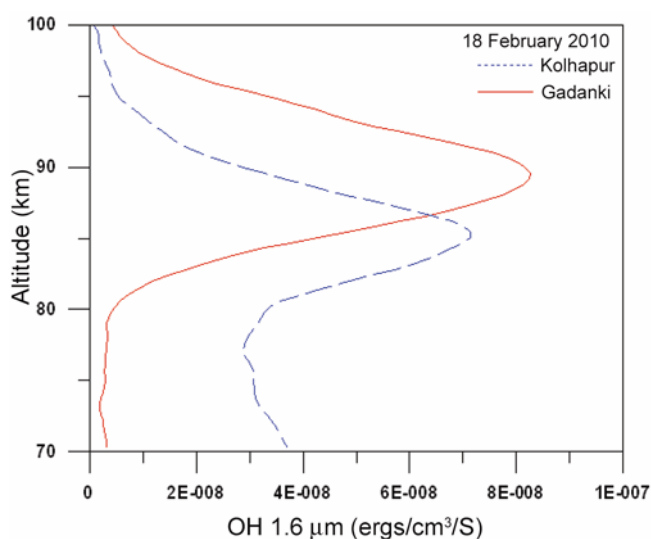


**Figure 5.** The OH emission profiles obtained by the SABER instrument on-board Thermosphere Ionosphere Mesosphere Energetic and Dynamics satellite mission corresponding to the locations Kolhapur and Gadanki (source: <http://saber.gats-inc.com/>).

1. Takahashi, H., Buriti, R. A., Gobbi, D. and Batista, P. P., Equatorial planetary wave signatures observed in mesospheric airglow emissions. *J. Atmos. Sol. Terr. Phys.*, 2002, **64**, 1263–1272.
2. Taylor, M. J., Pendleton Jr, W. R., Gardner, C. S. and States, R. J., Comparison of terdiurnal tidal oscillations in mesospheric OH rotational temperature and Na lidar temperature measurements at mid-latitudes for fall/spring conditions. *Earth Planets Space*, 1999, **51**, 877–885.
3. Taori, A., Taylor, M. J. and Franke, S., Terdiurnal wave signatures in the upper mesospheric temperature and their association with the wind fields at low latitudes ( $20^\circ\text{N}$ ). *J. Geophys. Res.*, 2005, **110**, D09S06; doi: 10.1029/2004JD004564.
4. Takahashi, H., Batista, P. P., Buriti, R., Gobbi, A. D., Nakamura, T., Tsuda, T. and Fukao, S., Response of the airglow OH emission, temperature and mesopause wind to the atmospheric wave propagation over Shigaraki, Japan. *Earth Planets Space*, 1999, **51**, 863–875.
5. Taori, A. and Taylor, M., Characteristics of wave induced oscillations in mesospheric  $\text{O}_2$  emission intensity and temperatures. *Geophys. Res. Lett.*, 2006, **33**, L01813; doi: 10.1029/2005GL024442.
6. Taori, A., Guharay, A. and Taylor, M. J., On the use of simultaneous measurements of OH and  $\text{O}_2$  emissions to investigate wave growth and dissipation. *Ann. Geophys.*, 2007, **25**, 639–643.
7. Suzuki, S., Shiokawa, K., Otsuka, Y., Ogawa, T., Nakamura, K. and Nakamura, T., A concentric gravity wave structure in the mesospheric airglow images. *J. Geophys. Res.*, 2007, **112**, D02102; doi: 10.1029/2005JD006558.
8. Krassovsky, V. I., Infrasonic variation of OH emission in the upper atmosphere. *Ann. Geophys.*, 1972, **28**, 739–746.
9. Tarasick, D. W. and Hines, C. O., The observable effects of gravity waves in airglow emission. *Planet. Space Sci.*, 1990, **8**, 1105–1119.

10. Aushev, V. M., Lyahov, V. V., Lopez-Gonzalez, M. J., Shepherd, M. G. and Dryna, E. A., Solar eclipse of the 29 March 2006: results of the optical measurements by MORTI over Almaty (43.03°N, 76.58°E). *J. Atmos. Sol. Terr. Phys.*, 2008, **70**, 1088–1101.
11. Guharay, A., Taori, A., Bhattacharjee, B., Pant, P., Pande, P. and Pandey, K., First ground-based mesospheric measurements from central Himalayas. *Curr. Sci.*, 2009, **97**, 664–669.
12. Reisin, E. R. and Scheer, J., Vertical propagation of gravity waves determined from zenith observations of airglow. *Adv. Space Res.*, 2001, **27**, 1743–1748.
13. Reisin, E. R. and Scheer, J., Gravity wave activity in the mesopause region from airglow measurements at El Leoncito. *J. Atmos. Sol. Terr. Phys.*, 2004, **66**, 655–661.
14. Takahashi, H., Sahai, Y., Batista, P. P. and Clemesha, B. R., Atmospheric gravity wave effect on the airglow O<sub>2</sub> (0-1) and OH (9-4) band intensity and temperature variations observed from a low latitude station. *Adv. Space Res.*, 1992, **12**, 131–134.
15. Takahashi, H., Onohara, A., Shiokawa, K., Vargas, F. and Gobbi, D., Atmospheric wave induced O<sub>2</sub> and OH airglow intensity variations: effect of vertical wavelength and damping. *Ann. Geophys.*, 2011, **29**, 631–637.
16. Taylor, M. J., Gardner, L. C. and Pendleton Jr, W. R., Long-period wave signatures in mesospheric OH Meinel (6, 2) band intensity and rotational temperature at mid-latitudes. *Adv. Space Res.*, 2001, **27**, 1171–1179.
17. Viereck, R. A. and Deehr, C. S., On the interaction between gravity waves and the OH Meinel (6-2) and O<sub>2</sub> atmospheric (0-1) bands in the polar night airglow. *J. Geophys. Res.*, 1989, **94**, 5397–5404.
18. Reisin, E. R. and Scheer, J., Characteristics of atmospheric waves in the tidal period range derived from zenith observations of O<sub>2</sub> (0-1) atmospheric and OH (6-2) airglow at lower mid-latitudes. *J. Geophys. Res.*, 1996, **101**, 21223–21232.
19. Lopez-Gonzalez, M. J. *et al.*, Tidal variations of O<sub>2</sub> atmospheric and OH (6-2) airglow and temperature at mid-latitude from SATI observations. *Ann. Geophys.*, 2005, **23**, 3579–3590.
20. Ghodpage, R. N., Singh, D., Singh, R. P., Mukherjee, G. K., Vohat, P. and Singh, A. K., Tidal and gravity waves study from the airglow measurements at Kolhapur (India). *J. Earth Syst. Sci.*, 2012, **121** (in press).
21. Taori, A. and Parihar, N., Simultaneous bi-station measurements of mesospheric waves from Indian low latitudes. *J. Adv. Space Res.*, 2011, **48**, 218–226; doi: 10.1016/j.asr.2011.03.026.
22. Taori, A., Kamalakar, V., Raghunath, K., Rao, S. V. B. and Russell, J. M., Simultaneous Rayleigh lidar and airglow measurements of middle atmospheric waves over low latitudes in India. *J. Atmos. Sol. Terr. Phys.*, 2012, **78–79**, 62–69; doi: 10.1016/j.jastp.2011.06.012.
23. Meriweather, J. W., Ground based measurements of mesospheric temperatures by optical means. In *International Council of Scientific Unions Middle Atmosphere Program Handbook* (ed. Vincent, R.), USA, NASA, 1984, vol. 13, pp. 1–18.
24. Hines, C. O. and Tarasick, D. W., On the detection and utilization of gravity waves in airglow studies. *Planet. Space Sci.*, 1987, **35**, 851–866.
25. Walterscheid, R. L., Schubert, G. and Hickey, M. P., Comparison of theories for gravity wave fluctuations in airglow emissions. *J. Geophys. Res.*, 1994, **99**, 3935–3944.
26. Taori, A. and Taylor, M., Dominant winter-time mesospheric wave signatures over a low latitude station, Hawaii (20.8 1N): an investigation. *J. Earth Syst. Sci.*, 2010, **119**, 259–264.
27. Hickey, M. P., Schubert, G. and Walterscheid, R. L., Gravity wave driven fluctuations in the O<sub>2</sub> atmospheric (0-1) nightglow from an extended, dissipative emission region. *J. Geophys. Res.*, 1993, **98**, 13717–13729.
28. Walterscheid, R. L. and Schubert, G., A dynamical–chemical model of fluctuations in the OH airglow driven by migrating tides, stationary tides and planetary waves. *J. Geophys. Res.*, 1995, **100**, 17443–17449.
29. Guharay, A., Taori, A. and Taylor, M., Summer-time nocturnal wave characteristics in mesospheric OH and O<sub>2</sub> airglow emissions. *Earth Planets Space*, 2008, **60**, 973–979.
30. Offermann, D., Friedrich, V., Ross, P. and von Zahn, U., Neutral gas composition measurements between 80 and 120 km. *Planet. Space Sci.*, 1981, **29**, 747–764.
31. Makhlof, U. B., Picard, R. H. and Winick, J. R., Photochemical–dynamical modeling of the measured response of airglow to gravity waves, 1: basic model for OH airglow. *J. Geophys. Res.*, 1995, **100**, 11289–11311.
32. Hines, C. O. and Tarasick, D. W., Layer truncation and the Eulerian/Lagrangian duality in the theory of airglow fluctuations induced by gravity waves. *J. Atmos. Sol. Terr. Phys.*, 1997, **59**, 327–334.
33. Schubert, G., Walterscheid, R. L. and Hickey, M. P., Gravity wave-driven fluctuations in OH nightglow from an extended, dissipative emission region. *J. Geophys. Res. A*, 1991, **96**, 13869–13880.

ACKNOWLEDGEMENTS. This work is carried out under the research grant funded by the Ministry of Science and Technology and the Department of Space, Government of India. The night airglow observations at Kolhapur were carried out under the scientific collaboration between the Indian Institute of Geomagnetism, Mumbai and the Shivaji University, Kolhapur. The SABER data were downloaded from <http://saber.gats-inc.com/>.

Received 31 May 2012; revised accepted 14 November 2012

## Past and General Circulation Model-driven future trends of climate change in Central Indian Punjab: ensuing yield of rice–wheat cropping system

S. K. Jalota<sup>1\*</sup>, Harsimran Kaur<sup>1</sup>, S. S. Ray<sup>2</sup>, R. Tripathy<sup>2</sup>, B. B. Vashisht<sup>1</sup> and S. K. Bal<sup>3</sup>

<sup>1</sup>Department of Soil Science and <sup>3</sup>Department of Agro-Meteorology, Punjab Agricultural University, Ludhiana 141 004, India

<sup>2</sup>Agro-Ecosystems Division, Space Applications Centre, Ahmedabad 380 015, India

**Climate data recorded for the last 40 years (1971–2010) at meteorological station of Punjab Agricultural University, Ludhiana (Central Indian Punjab) and future changes in climate data derived from three General Circulation Models (GCMs), viz. HadCM3, CSIRO-Mk2 and CCCMA-CGCM2, were analysed. Past data showed increase in temperature, decrease in open pan evaporation and irregular trends in rainfall. Amongst GCMs, the HadCM3 model showed rela-**

\*For correspondence. (e-mail: jalotask03@yahoo.com)